the journal of biological chemistry

jbc

JULY 10, 2015
VOLUME 290
NUMBER 28

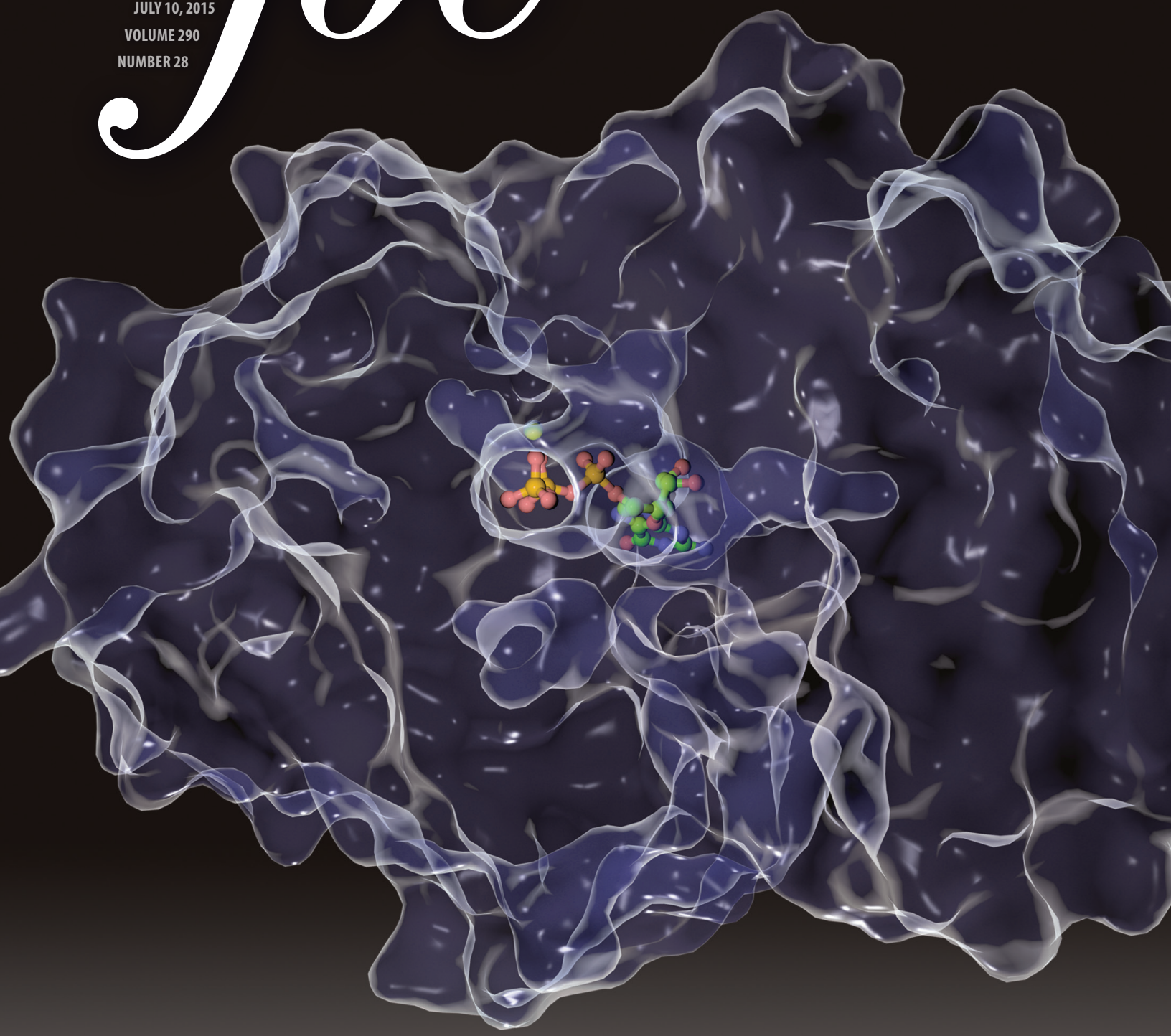

ASBMB AMERICAN SOCIETY FOR BIOCHEMISTRY AND MOLECULAR BIOLOGY

THE JOURNAL OF BIOLOGICAL CHEMISTRY VOL. 290, NO. 28, pp. 17085–17095, July 10, 2015

Integration of Fourier Transform Infrared Spectroscopy, Fluorescence Spectroscopy, Steady-state Kinetics and Molecular Dynamics Simulations of $G\alpha_{i1}$ Distinguishes between the GTP Hydrolysis and GDP Release Mechanism*

Received for publication, March 10, 2015, and in revised form, May 8, 2015 Published, JBC Papers in Press, May 15, 2015, DOI 10.1074/jbc.M115.651190

Grit Schröter[1], **Daniel Mann**[1], **Carsten Kötting**[2], **and Klaus Gerwert**[3]

From the Biophysics Department, Ruhr-University Bochum, 44801 Bochum, Germany

Background: Multiple turnover GTPase assays of Gα are dominated by nucleotide exchange.
Results: FTIR elucidates single turnover rates and individual phosphate vibrations.
Conclusion: $G\alpha_{i1}$-R178S is slowed down in single turnover hydrolysis by 2 orders of magnitude, $G\alpha_{i1}$-Asp^{229} and -Asp^{231} are key players in Ras-like/all-α domain coordination.
Significance: With FTIR on Gα established, detailed information on the reaction mechanism can be obtained.

Gα subunits are central molecular switches in cells. They are activated by G protein-coupled receptors that exchange GDP for GTP, similar to small GTPase activation mechanisms. Gα subunits are turned off by GTP hydrolysis. For the first time we employed time-resolved FTIR difference spectroscopy to investigate the molecular reaction mechanisms of $G\alpha_{i1}$. FTIR spectroscopy is a powerful tool that monitors reactions label free with high spatio-temporal resolution. In contrast to common multiple turnover assays, FTIR spectroscopy depicts the single turnover GTPase reaction without nucleotide exchange/Mg^{2+} binding bias. Global fit analysis resulted in one apparent rate constant of 0.02 s^{-1} at 15 °C. Isotopic labeling was applied to assign the individual phosphate vibrations for α-, β-, and γ-GTP (1243, 1224, and 1156 cm^{-1}, respectively), α- and β-GDP (1214 and 1134/1103 cm^{-1}, respectively), and free phosphate (1078/991 cm^{-1}). In contrast to Ras·GAP catalysis, the bond breakage of the β-γ-phosphate but not the P_i release is rate-limiting in the GTPase reaction. Complementary common GTPase assays were used. Reversed phase HPLC provided multiple turnover rates and tryptophan fluorescence provided nucleotide exchange rates. Experiments were complemented by molecular dynamics simulations. This broad approach provided detailed insights at atomic resolution and allows now to identify key residues of $G\alpha_{i1}$ in GTP hydrolysis and nucleotide exchange. Mutants of the intrinsic arginine finger ($G\alpha_{i1}$-R178S) affected exclusively the hydrolysis reaction. The effect of nucleotide binding ($G\alpha_{i1}$-D272N) and Ras-like/all-α interface coordination ($G\alpha_{i1}$-D229N/$G\alpha_{i1}$-D231N) on the nucleotide exchange reaction was furthermore elucidated.

Heterotrimeric G proteins are interaction partners of G protein-coupled receptors (GPCRs)[4] and deliver external signals into the cell (1). They are switched on by exchange of GDP for GTP induced by the GPCR as exchange factor and switched off by GTP hydrolysis. The nucleotide is bound between two domains of the Gα-subunit, namely the Ras-like domain, which is similar to the G-domain of small GTPases, and the all-α domain. In its inactive state $G\alpha_{i1}\beta\gamma$ exists GDP bound in its heterotrimeric form. Activation by guanosine nucleotide exchange factors, like GPCRs or non-receptor guanosine nucleotide exchange factors (2–4), leads to nucleotide exchange in the α-subunit. Incorporation of GTP alters the protein conformation in the switch I-III regions (5), which causes separation of the $G\alpha_{i1}$ and $\beta\gamma$ subunits and signal transduction, *e.g.* by binding of $G\alpha_{i1}$ to adenylate cyclase isoforms that in turn inhibit the production of cAMP from ATP (6). GTPase activity of $G\alpha_{i1}$ leads to hydrolysis of GTP to GDP and P_i, inactivation, and reassociation with its $\beta\gamma$ subunits. Heterotrimeric G proteins are equipped with an intrinsic arginine finger (Arg^{178} in $G\alpha_{i1}$) usually provided in case of small GTPases by the GAP protein, which is known to function as a key residue for catalyzing the hydrolysis reaction. Therefore intrinsic GTPase rates of $G\alpha_{i1}$ are rather comparable with Ras·GAP than to Ras. The hydrolysis mechanism taking place in $G\alpha_{i1}$ thereby determines the duration of its active state, which can be pathogenic when hindered, *e.g.* by ADP-ribosylation catalyzed by pertussis toxin (7). As for Ras, the intrinsic hydrolysis activity of $G\alpha_{i1}$ can be further accelerated by GTPase activating proteins (GAPs), which are called regulators of G protein signaling (RGS), *e.g.* RGS4 in case of $G\alpha_{i1}$ (8). It is generally known that GDP/GTP exchange is the rate-limiting step in multiple turnover measurements of Gα isoforms (9–12). Therefore, beside steady-state assays using γ-^{32}P labeling (13) or malachite green (14), pre-steady-state assays are used to characterize the hydrolysis reaction of Gα

* This work was supported by Deutsche Forschungsgemeinschaft Grant SFB 642, TP A1. The authors declare that they have no conflicts of interest with the contents of this article.
[1] Both authors are considered co-first authors.
[2] To whom correspondence may be addressed: Universitätsstr. 150, 44801 Bochum, Germany. Tel.: 49-234-3224873; Fax: 49-234-3204873; E-mail: carsten.koetting@rub.de.
[3] To whom correspondence may be addressed: Universitätsstr. 150, 44801 Bochum, Germany. Tel.: 49-234-3224461; Fax: 49-234-3214238; E-mail: klaus.gerwert@bph.rub.de.

[4] The abbreviations used are: GPCR, G protein-coupled receptor; GAP, GTPase activating protein; pHP, para-hydroxyphenacyl; NPE, 1-*ortho*-nitrophenyl ethyl; GTPγS, guanosine 5′-3-*O*-(thio)triphosphate; RGS, regulators of G protein signaling; MD, molecular dynamics; PDB, Protein Data Bank.

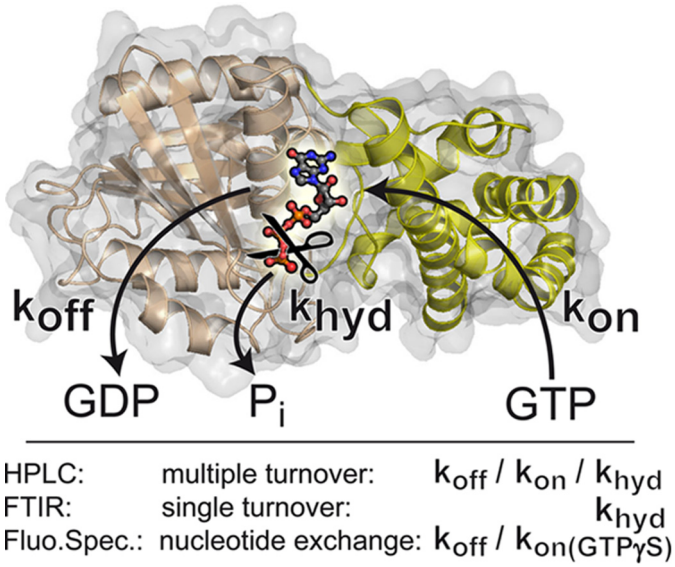

FIGURE 1. **$G\alpha_{i1}$ is switched on by the exchange of GDP for GTP (k_{off}/k_{on}), then GTP hydrolysis proceeds (k_{hyd}) and P_i is released.** Multiple turnover kinetics were measured via HPLC, which cannot distinguish between the three processes. Nucleotide exchange kinetics (k_{off}/k_{on}) were monitored via tryptophan fluorescence spectroscopy. Single turnover kinetics (k_{hyd}) were measured via time-resolved FTIR difference spectroscopy.

isoforms (15–18). We present here for the first time single turnover measurements of $G\alpha_{i1}$ using time-resolved FTIR spectroscopy, an ultrasensitive method that can be applied in solution and has been successfully used for photoactivable proteins like bacteriorhodopsin (19, 20), channelrhodopsin (21), and other rhodopsins (22). Adenylyltransferases (23), ATPases (24–27), and GTPases (28–31) can also be investigated by usage of caged nucleotides (28). The resulting photolysis and hydrolysis difference spectra depict the label-free GTP and GDP states of $G\alpha_{i1}$ and are able to reflect environmental changes in the sub-Å range (32) and the dynamics at a time resolution of milliseconds. Bridging the gap between single turnover and steady-state kinetics, we also applied a multiple turnover GTPase assay using reversed phase HPLC and additionally measured the nucleotide exchange rate using tryptophan fluorescence of Trp^{211} at 280/340 nm as extensively described elsewhere (15, 18, 33) and molecular dynamics simulations. GDP release and GTP uptake is a complex mechanism determined by the movement of the all-α domain, which was shown by structural studies (34). The Ras-like/all-α interface thereby depicts a complex interaction network including both amino acids and the nucleotide. By orchestration of different methods we were able to determine the effect of point mutations and distinguish their role in hydrolysis and nucleotide exchange.

Materials and Methods

$G\alpha_{i1}$-WT and mutant proteins were expressed, isolated, and characterized by various biophysical and biochemical methods (Fig. 1).

Michaelis-Menten multiple turnover kinetics were monitored via reversed phase HPLC. The kinetics include both the catalytic reaction and the dissociation/association kinetics depicted as time per turnover. The isolated single turnover hydrolysis reaction was obtained via FTIR spectroscopy as half-life values of the global fit. The isolated nucleotide exchange kinetics were investigated via tryptophan fluorescence spectroscopy and depicted as half-life values of the intensity change. Experiments were accompanied by molecular dynamics simulations to decode the molecular reactions at the atomic level.

Chemicals—Lyophilized GDP, GTP, and GTPγS were purchased from Jena Bioscience (Jena, Germany). The photolabeled nucleotide *para*-hydroxyphenacyl (pHP) cgGTP and the isotopologues α-$^{18}O_2$- and β-$^{18}O_3$-pHPcgGTP were synthesized as described previously (29, 35–37). 1-*Ortho*-nitrophenyl ethyl (NPE) cgGTP and γ-$^{18}O_4$-NPEcgGTP were synthesized as described previously (38). Alkaline phosphatase coupled to agarose beads was purchased from Sigma (Munich, Germany).

Cloning—The gene for the human GNAI1 (UniProtKB accession number P63096-1; kind gift from C. Wetzel, University of Regensburg, Germany (39)) was amplified by polymerase chain reaction using the oligonucleotide primers GCGCCCATGGGCTGCACGCTGAGC and GCGCGGATCCTTAAAAGAGACCACAATCTTTTAG (restriction sites for NcoI and BamHI are underlined). Resulting fragments were cut with NcoI and BamHI and ligated into the vector pET27bmod (kind gift from M. Engelhard, MPI Dortmund, Germany (40)) with a N-terminal ×10 histidine tag and tobacco etch virus (TEV) site. The plasmid was transformed into *Escherichia coli* DH5α for amplification. $G\alpha_{i1}$ mutants R178S, D229N, D231N, and D272N were created by overlap PCR using appropriate primers. Integrity of each construct was confirmed by sequencing. cDNA encoding human RGS4 was acquired from the Missouri cDNA Resource Center (Rolla, MO), tagged with a N-terminal ×10 histidine tag and TEV site, and also ligated into the vector pET27bmod. Amplification was performed similar to $G\alpha_{i1}$.

Protein Expression—The plasmid encoding $G\alpha_{i1}$ was transformed into *E. coli* Rosetta 2 (DE3) (Novagen®, Merck, Darmstadt, Germany) and incubated overnight at 37 °C on LB agar plates containing 0.2% (w/v) glucose as well as 50 μg/ml of kanamycin and 20 μg/ml of chloramphenicol for plasmid and strain selection. A preculture (LB medium, 50 μg/ml of kanamycin, 20 μg/ml of chloramphenicol, 0.2% (w/v) glucose) was inoculated and incubated overnight at 37 °C and 160 rpm. The plasmid encoding RGS4 was transformed into *E. coli* BL21(DE3) under identical conditions using only kanamycin for plasmid selection. For the main culture, 18 liters of LB medium supplemented with 50 μg/ml kanamycin and 0.2% glucose were inoculated with the preculture and grown at 37 °C, 100 rpm, and 20 liters/min airflow in a Biostat® C20-3 Fermenter (Sartorius, Göttingen, Germany). At an A_{600} of 0.5–0.6 the culture was cooled to 18 °C and protein expression was induced by addition of 0.25 mM isopropyl 1-thio-β-D-galactopyranoside. After 15–18 h the cells were harvested by centrifugation at 5000 × *g* and 4 °C, suspended in buffer A (20 mM Tris, pH 8, 300 mM NaCl, 1 mM $MgCl_2$, 0.5 mM EDTA, 5 mM D-norleucine for $G\alpha_{i1}$ or 50 mM Tris, pH 8, 150 mM NaCl, 0.5 mM EDTA, 5 mM D-norleucine for RGS4), flash frozen, and stored at −80 °C.

Protein Isolation—Frozen cells were thawed, supplemented with 0.3 mM PMSF, 5 mM β-mercaptoethanol, DNase ($G\alpha_{i1}$ containing cells were additionally supplemented with 0.1 mM GDP), and disrupted using a microfluidizer M-110L (Microflu-

idics Corp., Newton, MA) at 800 bar. To spin down cell fragments and not disrupted cells, the suspension was centrifuged for 45 min at 45,000 × *g* and 4 °C. RGS4 containing cells were centrifuged with an additional low-speed step for 15 min at 18,000 × *g* and 4 °C followed by high-speed centrifugation for 45 min at 75,000 × *g* and 4 °C. The supernatant was applied to a 25-ml nickel-nitrilotriacetic acid superflow (Qiagen, Hilden, Germany) column, equilibrated with buffer B (buffer A + 0.3 mM PMSF + 5 mM β-mercaptoethanol + 20 mM imidazole), using a ÄKTApurifier 100 system (GE Healthcare Life Sciences, Freiburg, Germany) at 6 °C with a flow rate of 1–2 ml/min. After a washing step with buffer C (buffer B + 4 mM $MgCl_2$, 400 mM KCl, 1 mM ATP) for 8–10 column volumes and a subsequent step with buffer B + 50 mM imidazole for another 8–10 column volumes, the proteins were eluted with buffer B + 200 mM imidazole. The fractions containing $G\alpha_{i1}$ or RGS4 were selected after SDS-PAGE, pooled, supplemented with 5 mM DTT, and concentrated to 5 ml using a 10,000 MWCO concentrator (Amicon Ultra-15, Merck Millipore, Darmstadt, Germany). For gel filtration chromatography, the pool was applied to an illustra HiLoad 26/600 Superdex 200 pg column (GE Healthcare Life Sciences, Freiburg, Germany) equilibrated with buffer D (20 mM Tris, pH 8, 300 mM NaCl, 1 mM $MgCl_2$, 2 mM DTT, 0.1 mM GDP for $G\alpha_{i1}$ or 50 mM Hepes, pH 8, 100 mM KCl, 2 mM DTT for RGS4). Peak fractions were analyzed by SDS-PAGE. Purest fractions containing $G\alpha_{i1}$ or RGS4 were mixed 1:2 with buffer E (20 mM Tris, pH 8, 1 mM $MgCl_2$, 0.1 mM GDP for $G\alpha_{i1}$ or 50 mM Hepes, pH 8, 100 mM KCl for RGS4), pooled, and concentrated to ~20 mg/ml for $G\alpha_{i1}$ or ~10 mg/ml for RGS4 using a 10,000 MWCO concentrator. Protein concentration was determined using Bradford reagent as triplicate. The concentrated pool was aliquoted, flash frozen, and stored at −80 °C until utilization. Coomassie-stained gels after SDS-PAGE of purified proteins are depicted in Fig. 2.

Multiple Turnover GTPase Measurements—For determination of the GTPase activity under multiple turnover conditions, the samples contained 10 μM $G\alpha_{i1}$ in 20 mM Tris, pH 8, 150 mM NaCl, 0.5 mM $MgCl_2$, and 0.1 mM DTT. After tempering for 5 min at 30 °C, 0.1 mM GTP ($G\alpha_{i1}$-WT, -R178S, -D229N, -D231N) or 2.5 mM GTP ($G\alpha_{i1}$-D272N) was added and immediately the first aliquot of the sample was analyzed by reversed phase HPLC at 254 nm (Beckman Coulter System Gold, Pasadena CA) (mobile phase: 50 mM P_i, pH 6.5, 5 mM tetrabutylammonium bromide, 7.5% AcN; stationary phase: ODS-Hypersil C18 column). After a 10-min incubation at 30 °C, a second aliquot was analyzed by HPLC. The amount of GTP was chosen to guarantee a substantial excess of GTP during the whole time of the measurements. Evaluation of the data were done by integration of the GDP and GTP peaks followed by normalization (sum of the areas $A_{GDP} + A_{GTP} = 1$). Determination of the time for one turnover per molecule $G\alpha_{i1}$, including exchange of GDP for GTP and GTP hydrolysis, was done according to the calculation of turnover times formula,

$$\frac{\text{time [min]}}{\text{turnover}} = \frac{(t_1 - t_0)}{(A_{GTP,t_0} - A_{GTP,t_1}) \cdot \frac{c(GTP)}{c(G\alpha_{i1})}} \qquad \text{(Eq. 1)}$$

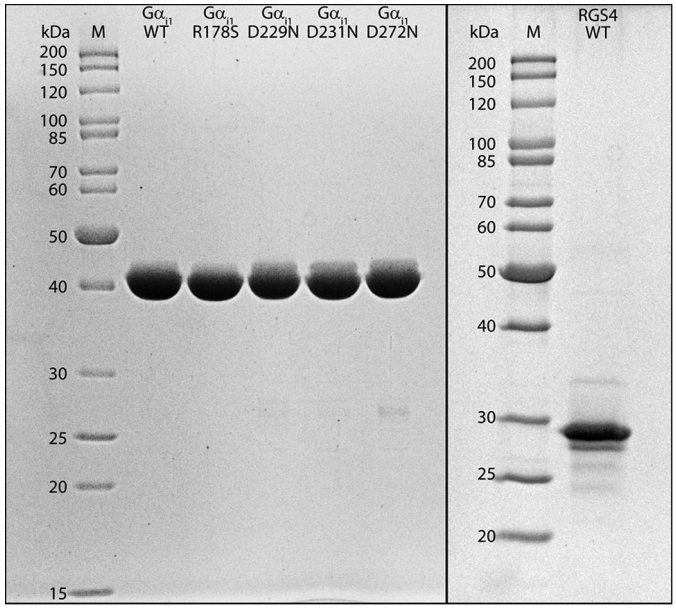

FIGURE 2. **SDS-PAGE of wild type and mutant $G\alpha_{i1}$ and wild type RGS4 proteins after purification.** 2.5 μg of wild type and mutant $G\alpha_{i1}$ and wild type RGS4 was loaded on a 12.5% polyacrylamide SDS gel together with Page Ruler Unstained Protein Ladder (Thermo Fisher Scientific, Waltham, MA) as size standard. Chromatography runs were performed with 60 mA for 30 min and staining was performed using Coomassie Brilliant Blue.

with time points t_0 and t_1 [min], the areas of the GTP peak at the time points t_0 and t_1 $A_{GTP,t0}$ and $A_{GTP,t1}$ (normalized area), and the concentration of $G\alpha_{i1}$ and GTP c($G\alpha_{i1}$/GTP). Calculated values were averaged and the standard deviation was calculated from three experiments for each wild type and mutant protein.

Monitoring the Nucleotide Exchange Rate Using Fluorescence Spectroscopy—The nucleotide exchange rate of wild type and mutant $G\alpha_{i1}$ was measured via tryptophan fluorescence of Trp^{211} (41, 42) using a Jasco FP 6500 Spectrofluorometer (Easton, MD). 500 nM wild type or mutant protein was supplemented with 20 mM Tris, pH 8, 150 mM NaCl, 1 mM $MgCl_2$, and 1 mM DTT and tempered 5 min to 30 °C. After monitoring the fluorescence baseline for another 5 min, nucleotide exchange was initiated by the addition of 2.5 μM GTPγS and the reaction was monitored with λ_{exc} = 280 nm and λ_{em} = 340 nm for at least 60 min. Mixing was ensured by constant stirring with a stirring bar and the temperature was controlled by an external water bath.

Data were fitted in OriginPro 9 (OriginLab Corp., Northampton, MA) using a monoexponential formula with a linear correction, which accounts for bleaching,

$$I = a \times e^{-kt} + m \times t + n \qquad \text{(Eq. 2)}$$

with the rate constant *k*, the amplitude coefficient *a*, the slope *m*, and the offset *n*. Half-life values were calculated using ($t_{½}$ = ln(2)/*k*). Half-life values were averaged and the standard deviation was calculated from three experiments for each wild type and mutant protein.

Nucleotide Exchange of Wild Type and Mutant $G\alpha_{i1}$ to Caged GTP—The exchange of bound GDP to photolabile pHPcgGTP or NPEcgGTP was performed in the presence of alkaline phosphatase coupled to agarose beads, which is unable to hydrolyze

caged compounds. Phosphatase beads were washed 5 times in buffer 1 (50 mM Tris, pH 7.5, 100 μM $ZnSO_4$) to remove free phosphatase. Each washing step was followed by centrifugation at 10,000 × *g* and the supernatant was checked for free phosphatase using a colorimetric assay with *para*-nitrophenylphosphate (43). 5 mg of wild type or mutant $G\alpha_{i1}$ were supplemented with 50 mM Tris, pH 7.5, 10 μM $ZnSO_4$ and a 2× molar excess of the caged nucleotide. Hydrolysis of free and protein-bound GDP to guanosine was monitored via HPLC. After 3 h at room temperature >95% of GDP was hydrolyzed. Samples were centrifuged at 10,000 × *g* for 2 min and the supernatant was re-buffered through a Nap5 column (GE Healthcare Life Sciences) that was equilibrated with 10 mM Hepes, pH 7.5, 7.5 mM NaCl, 0.25 mM $MgCl_2$, 1 mM DTT at 7 °C. Protein fractions were pooled and concentrated in a 10,000 MWCO concentrator (Amicon Ultra-0.5, Merck Millipore, Darmstadt, Germany). Concentrations were determined using Bradford reagent as triplicate and the nucleotide exchange rate of bound caged nucleotide was again determined via HPLC (>95%). Samples were aliquoted into 107.5 μg portions (5 mM final concentration in FTIR measurements), flash frozen in liquid nitrogen, and stored at −80 °C. Subsequently samples were lyophilized for 3 h at −55 °C/0.05 mbar in a Christ Alpha-1–2 LDPlus Lyophilizer (Martin Christ GmbH, Osterode am Harz, Germany) and stored light protected in parafilm and aluminum foil at −20 °C.

FTIR Measurements on $G\alpha_{i1}$—FTIR measurements were performed using 5 mM $G\alpha_{i1}$·cgGTP in 200 mM Hepes, pH 7.5, 150 mM NaCl, 5 mM $MgCl_2$, 20 mM DTT, 0.1% (v/v) ethylene glycol at 15 °C. RGS4 catalyzed measurements were performed by the addition of 5 mM RGS4 to establish a 1:1 complex with $G\alpha_{i1}$. Sample preparation was done under red light to protect the photolabile caged group. Composition of the required residual buffer depends on the protein concentration of the samples after nucleotide exchange to achieve the above named ion concentrations. FTIR samples were prepared between two CaF_2 windows (Ø 2 cm, 2 mm thickness, one of them with a 10-μm deepened area 1 cm in diameter). One lyophilisate of $G\alpha_{i1}$·cgGTP was dissolved in 0.5 μl of the appropriate residual buffer at the center of the deepened window and subsequently covered with the second window, whose rim had been lubricated with a thin ~1 mm wide silicon grease film. The windows were fixed in a metal cuvette and mounted in the spectrometer (Bruker IFS 66v/S or Vertex 80 v (Bruker, Ettlingen, Germany)). After sample equilibration, background spectra were taken (400 scans) and photolysis of the caged compounds was carried out with an LPX 240 XeCl excimer laser (Lambda Physics, Göttingen, Germany) by 12 flashes within 24 ms (pHPcgGTP) or 40 flashes within 80 ms (NPEcgGTP) at 308 nm (100–200 mJ/flash, 20 ns pulse duration) (28). Measurements were performed in the rapid-scan mode of the spectrometer for 30 min ($G\alpha_{i1}$-WT, -D229N, -D231N, -D272N) or 3 h ($G\alpha_{i1}$-R178S) using a liquid nitrogen-cooled mercury cadmium telluride detector. Data between 1800 and 950 cm^{-1} was collected with a spectral resolution of 4 cm^{-1} using an aperture of 5 mm in the double-sided forward-backward data acquisition mode with a scanner speed of 120 kHz. Data were analyzed via global fit (44). The absorbance change ($\Delta A(\nu,t)$) was fitted with a sum of exponential functions n describing the apparent rate constants k_1 and amplitudes a_1 of the hydrolysis reaction and the amplitudes a_0 of the photolysis reaction for every wavenumber ν.

$$\Delta A(\nu,t) = a_0(\nu) + \sum_{l=1}^{n} a_1(\nu)(1 - e^{-k_1 t}) \qquad \text{(Eq. 3)}$$

In the figures disappearing bands face downward and appearing bands face upward. Data were averaged over at least 3 measurements. Half-lives were calculated as arithmetic means, variation was calculated as standard deviations.

Molecular Dynamics Simulation and Evaluation—Molecular dynamics (MD) simulations were performed starting with the $G\alpha_{i1}$·Mg^{2+}·GTPγS structure of Protein Data Bank (PDB) code 1GIA (5) that depicts the truncated (Δ1–32 Δ345–354) active state of $G\alpha_{i1}$. Structure preparation was performed in Moby (45) and included correction of dihedrals, angles, and bonds according to the UA amber84 forcefield (46), protonation of ionizable side chains using the PKA,MAX,UH,JAB3 algorithm as well as replacement of the GTPγS for a GTP molecule (total charge: −4) and initial solvation by the Vedani algorithm (47). Point mutations were realized in Moby and were followed by a short headgroup optimization. Simulation systems were set up in GROMACS 4.0.7 (48–52). The prepared structures were thoroughly solvated in a cubic simulation cell filled with 154 mM NaCl in explicit TIP4P water. Simulations were carried out in the all atom OPLS forcefield (53) with GTP parameters from T. Rudack (54) at 310 K using the berendsen thermo- and barostat and a time step of 1 fs. Long range electrostatics were calculated using PME (cutoff 0.9 nm), short range electrostatics were calculated using a VDW cutoff of 1.4 nm. Bonds were constrained using LINCS. Systems were energy minimized and equilibrated for 25 ps with restrained protein positions followed by three free MD runs, each to a simulation time of 100 ns (total simulation time 1.5 μs).

Structure analysis was performed using the GROMACS evaluation tools and the contact matrix algorithm implemented in Moby. Pictures were created using PyMOL 1.7.1.1 (Schrödinger LLC, Portland, OR) and Gnuplot 4.4 (55).

Results

FTIR Measurements of $G\alpha_{i1}$—Time-resolved FTIR spectroscopy enables label-free detection of the GTP/GDP vibrations as well as determination of the apparent kinetics of the hydrolysis reaction. The protein was loaded with caged GTP and the sample was excited at 308 nm with a laser flash to remove the caged group (28) that cleaves rapidly (10^7 s^{-1} for pHPcgGTP (36)). The resulting difference spectrum is referred to as photolysis spectrum. Subsequently the intrinsic hydrolysis reaction in $G\alpha_{i1}$ takes place (Fig. 3).

The reaction (Scheme 1) is observed in FTIR. Global fit analysis of the absorbance changes revealed a monoexponential function that describes the hydrolysis (Fig. 4). No intermediate enrichment was observed in the measurements of $G\alpha_{i1}$-WT. Global fit analysis of five independent $G\alpha_{i1}$-WT measurements at 15 °C resulted in a half-life of 32.7 ± 2.5 s (k_{hyd} = 0.02 s^{-1}).

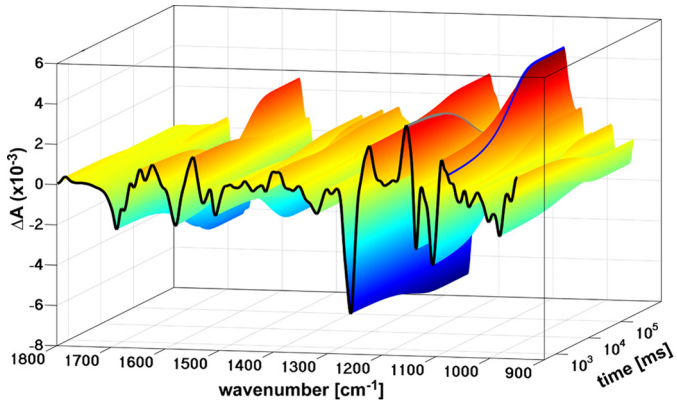

FIGURE 3. **Three-dimensional spectrum (global fit) of $G\alpha_{i1}$-WT.** The first spectrum represents the photolysis spectrum, subsequently hydrolysis takes place and was monitored. Time dependence of the bands at 1155 cm^{-1} (*gray*) and 1078 cm^{-1} (*blue*) is indicated. The absorbance change of these bands is shown in Fig. 4.

$$G\alpha\cdot cgGTP \xrightarrow[\text{photolysis}]{} G\alpha\cdot GTP \xrightarrow[\text{hydrolysis}]{} G\alpha\cdot GDP+P_i$$

SCHEME 1. **Reaction scheme observed in FTIR measurements.**

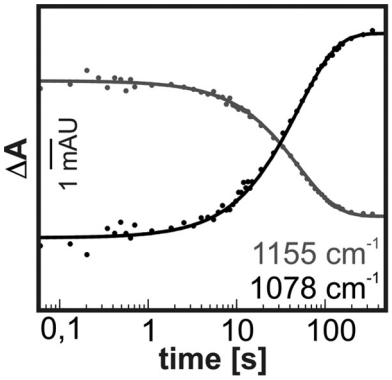

FIGURE 4. **Kinetics of FTIR measurements of the hydrolysis reaction in $G\alpha_{i1}$ at 15 °C on the basis of the bands for disappearing γ-GTP (1155 cm^{-1}) and appearing as free phosphate (1078 cm^{-1}) (see band assignment (Fig. 6)).** *Solid lines* represent the monoexponential global fit, *dots* represent data points.

Data analysis according to Equation 3 resulted in photolysis and hydrolysis spectrums that represent the transition from the pHPcgGTP to the GTP bound active state of $G\alpha_{i1}$ and the transition from the active GTP bound state to the inactive GDP bound state, respectively. Bands facing downward represent the educt state, bands facing upward represent the product state. Both spectra show numerous highly reproducible bands in the protein (1680–1350 cm^{-1}) and the phosphate (1350–950 cm^{-1}) region (Fig. 5). Surprisingly a band at 1784 cm^{-1} appeared in the photolysis and disappeared in the hydrolysis reaction, indicating a protonation of a carboxyl group from an Asp or Glu (56) in the GTP state (Fig. 5). To our knowledge this is the first time a protonation change has been observed in GTPases. For a clear cut assignment further studies with site-directed mutations have to be performed.

Phosphate vibrations were assigned using isotopically labeled nucleotides, namely α-$^{18}O_2$-pHPcgGTP, β-$^{18}O_3$-pHPcgGTP, and γ-$^{18}O_4$-NPEcgGTP. Double difference spectra of FTIR measurements using unlabeled and labeled nucleotides showed exclusively band shifts caused by the isotopes and allow

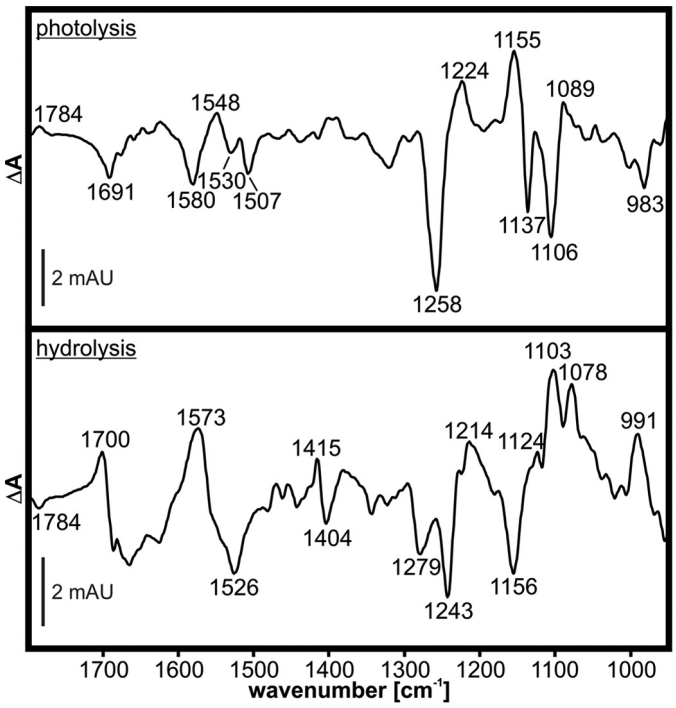

FIGURE 5. **Photolysis and hydrolysis spectrum of $G\alpha_{i1}$.** Bands *facing downward* in the photolysis spectrum represent the pHPcgGTP state of $G\alpha_{i1}$, bands *facing upward* depict the GTP bound state. Bands *facing downward and upward* in the hydrolysis spectrum represent the educt and product state of the hydrolysis reaction that takes place in $G\alpha_{i1}$, respectively. The spectral region between 1680 and 1620 cm^{-1} is superimposed by water absorptions and not further regarded.

band assignments of the phosphate region. In the photolysis spectrum the bands at 1240, 1224, and 1155 cm^{-1} were assigned to the asymmetric stretching vibrations of α-, β-, and γ-GTP (Fig. 6, *A* and *B*). The vibrations for β- and γ-GTP appear as clear bands, the α-band appears as a shoulder only in the photolysis spectrum but is more distinct in the hydrolysis spectrum. Band assignments of the hydrolysis reaction confirmed α-, β-, and γ-GTP vibrations at 1243, 1224, and 1156 cm^{-1}. The vibrations of the product state were assigned to 1214 cm^{-1} for α-GDP, 1134 and 1103 cm^{-1} for β-GDP, and 1078 and 991 cm^{-1} for the cleaved free phosphate (Fig. 6, *C* and *D*). The cleaved phosphate is not protein bound, as the vibrations at 1078 and 991 cm^{-1} are typical for free phosphate. Protein-bound phosphate intermediates are blue-shifted, *e.g.* in case of Ras·GAP an intermediate band appears at 1192 cm^{-1} (57). Because a protein-bound phosphate intermediate was not observed as in case of the Ras·GAP catalyzed reaction, bond breakage is the rate-limiting step in the hydrolysis reaction of $G\alpha_{i1}$ (Fig. 4). Summarizing, the hydrolysis reaction of $G\alpha_{i1}$-bound GTP to GDP and P_i was monitored label free at atomic resolution and in the millisecond time scale. Individual asymmetric stretching modes of GTP and GDP bound to $G\alpha_{i1}$ and P_i were assigned clear cut.

In addition, we performed the same experiments with the $G\alpha_{i1}$·RGS4 1:1 complex at 5 °C. Addition of RGS4 further catalyzed the hydrolysis reaction by almost 2 additional orders of magnitude (Fig. 7). As for the intrinsic measurements, global fit analysis resulted in one exponential rate, which demonstrates that again bond breakage is rate-limiting. No protein-bound

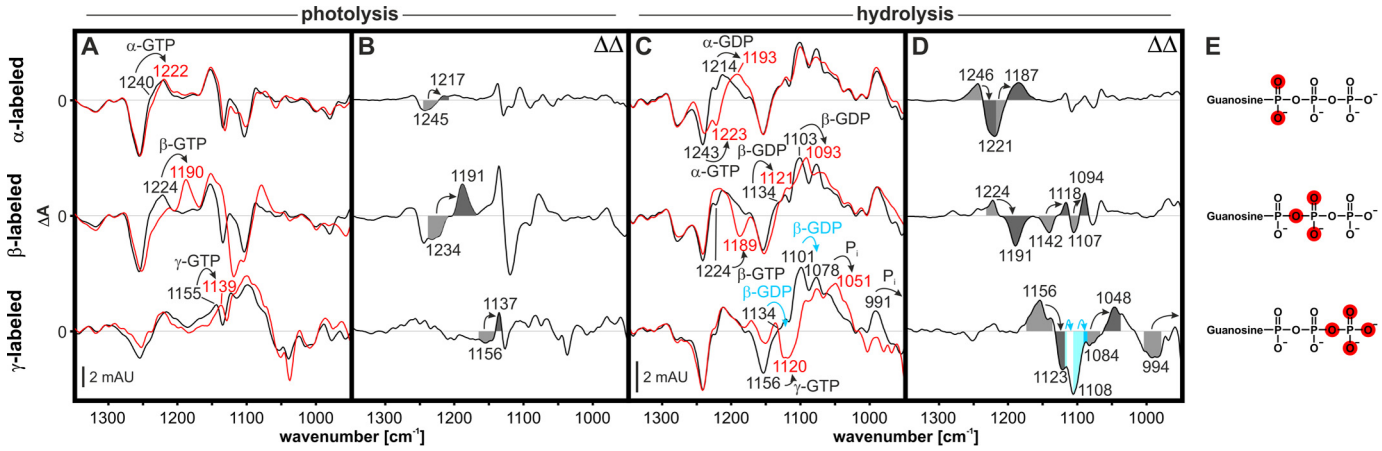

FIGURE 6. **Band assignment via isotopically labeled α-$^{18}O_2$-pHPcgGTP, β-$^{18}O_3$-pHPcgGTP, and γ-$^{18}O_4$-NPEcgGTP of the photolysis (*A*) and hydrolysis (*C*) reaction of Gα$_{i1}$ at 15 °C.** Measurements with NPEcgGTP were scaled by the factor of 5 (photolysis) or 10 (hydrolysis). *Arrows* indicate band shifts caused by the ^{18}O isotopes. Double differences (*B* and *D*) represent measurements with labeled minus unlabeled nucleotides and reveal the band shift only. The positions of ^{18}O labeling are depicted in *panel E*. The ^{18}O-labeled phosphoester in γ-$^{18}O_4$-NPEcgGTP leads to β-$^{18}O_1$-GDP, corresponding band shifts are marked in *cyan*.

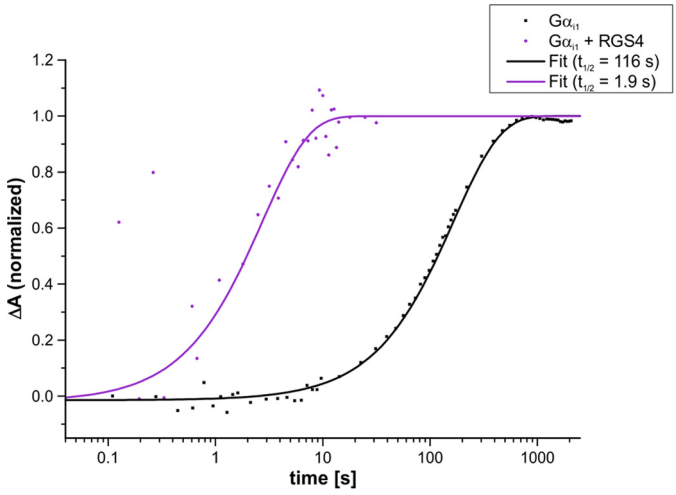

FIGURE 7. **Kinetics of the GTPase reactions of intrinsic Gα$_{i1}$ and Gα$_{i1}$·RGS4 measured via FTIR spectroscopy (β-GDP band at 5 °C)**

phosphate intermediate was observed and the absorptions of protein-bound GTP disappeared with the same rate as the absorptions of free P_i developed. RGS4 contributed numerous protein bands and altered the GTP/GDP binding modes. Assignments of these bands by isotopic labeling and site-specific mutagenesis will be part of future work.

In the following, various Gα$_{i1}$ residues were investigated to determine their role in nucleotide exchange and hydrolysis using site-directed mutagenesis. Investigations included the intrinsic arginine finger mutant Gα$_{i1}$-R178S that is known to have a slowed down hydrolysis rate (58), as well as mutations affecting the interface of the Ras-like and the all-α domain (Gα$_{i1}$-D229N/Gα$_{i1}$-D231N), and a residue that is participating in nucleotide binding (Gα$_{i1}$-D272N) (Fig. 8). Multiple turnover measurements via reversed phase HPLC, nucleotide exchange experiments via fluorescence spectroscopy, and single turnover measurements via time-resolved FTIR spectroscopy were used to investigate these mutants.

Steady-state Measurements—The multiple turnover GTPase reaction of wild type and mutant Gα$_{i1}$, consisting of nucleotide exchange ($k_{off,GDP}$ and $k_{on,GTP}$) and the hydrolysis rate k_{hyd}, was investigated by reversed phase HPLC at 30 °C according to Equation 1. Results can be grouped into four classes. One turnover is a cycle consisting of GDP release, GTP binding, and GTP hydrolysis that took 12.7 ± 0.2 min for Gα$_{i1}$-WT. The arginine finger mutant Gα$_{i1}$-R178S was slowed down to 29.6 ± 1.6 min per turnover. Gα$_{i1}$-D229N and -D231N shared an accelerated turnover time of 3.9 ± 0.03 min and Gα$_{i1}$-D272N was accelerated even more to 0.5 ± 0.02 min per turnover (Fig. 9*A*). It is generally accepted that the GDP release step is rate-limiting in multiple turnover measurements of Gα-proteins (59). To further investigate the underlying rate constants we additionally performed nucleotide exchange and single turnover hydrolysis experiments.

Nucleotide Exchange Experiments—In contrast to multiple turnover experiments, tryptophan fluorescence spectroscopy can monitor solely the nucleotide exchange reaction from GDP to GTPγS of Gα$_{i1}$ as Trp^{211} is sensitive for binding of the third phosphate group (Fig. 10). Hydrolysis cannot proceed as GTPγS is a non-hydrolyzable GTP analogue. The results of nucleotide exchange can be grouped into three classes. In contrast to multiple turnover measurements, the half-life value for nucleotide exchange to GTPγS of Gα$_{i1}$-R178S was similar to Gα$_{i1}$-WT (12.8 ± 0.9 and 10.7 ± 0.2 min, respectively). Nucleotide exchange was accelerated by a factor of about 3 in Gα$_{i1}$-D229N and -D231N to 3.3 ± 0.2 and 3.7 ± 0.1 min and even more accelerated in Gα$_{i1}$-D272N (0.8 ± 0.03 min) (Fig. 9*B*). Hence it can be concluded that the acceleration in multiple turnover measurements of Gα$_{i1}$-D229N, -D231N, and -D272N can be explained by accelerated dissociation times for GDP and/or association times for GTP. On the other hand the decelerated multiple turnover time for Gα$_{i1}$-R178S is not caused by nucleotide exchange, indicating that nucleotide exchange is not the rate-limiting step for this mutant.

Single Turnover Hydrolysis Measurements Using FTIR—In contrast to multiple turnover measurements, time-resolved FTIR spectroscopy can determine the hydrolysis reaction label free under actual single turnover conditions with high spatio-temporal resolution. The half-life value was obtained from the

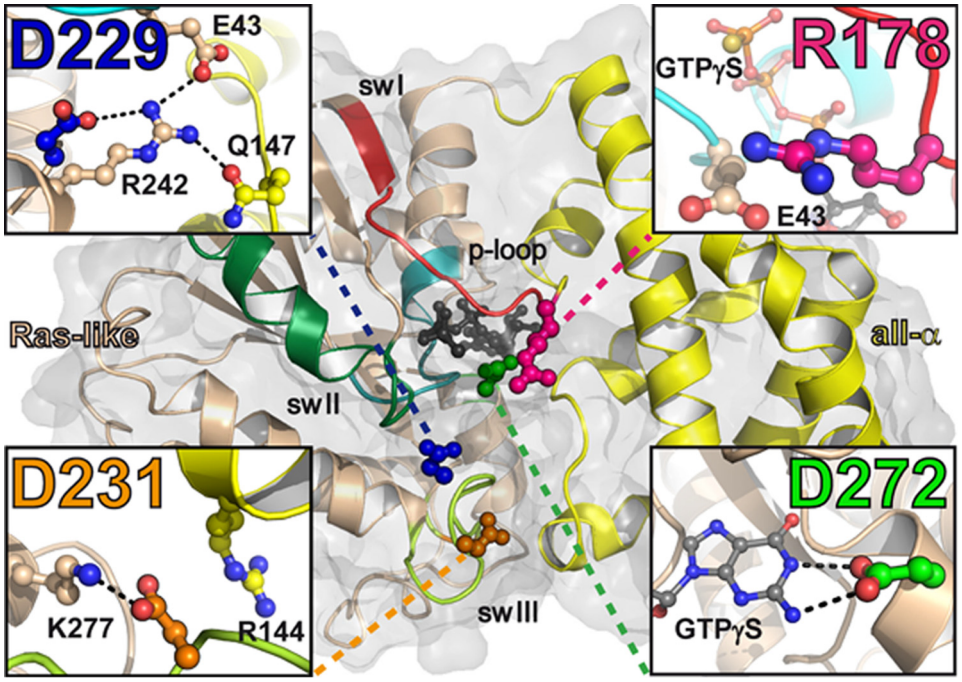

FIGURE 8. **Positions of the investigated mutants in $G\alpha_{i1}$ (PDB code 1GIA) (5).** The Ras-like domain is depicted in *beige*, the all-α domain in *yellow*, and the nucleotide in *gray*. Switch regions are colored *red* (switch I, residues 178–188), *dark green* (switch II, residues 202–218), and *light green* (switch III, residues 230–241). The p-loop (residues 40–47) is colored in *cyan*. Investigated mutants are located in the interface of the two domains (*D229*, *blue*; *D231*, *orange*), the phosphate binding region (*R178*, *magenta*), and the guanosine binding region (*D272*, *green*). Direct binding partners are colored by domain and by element; *black dashed lines* represent H-bonds. Switch definitions were adapted from Ref. 63. Colors of the mutants are retained hereafter.

results of the global fit procedure (44). The measured kinetics can again be grouped into three classes. $G\alpha_{i1}$-WT and $G\alpha_{i1}$-D231N had similar half-life values of 32.7 ± 2.5 and 27.8 ± 2.6 s, respectively. The single turnover hydrolysis reaction of $G\alpha_{i1}$-D229N and -D272N was slightly slowed down to 50.2 ± 4.5 or 49.8 ± 4.1 s. The hydrolysis reaction of $G\alpha_{i1}$-R178S was noticeably slowed down by 2 orders of magnitude to 3400 ± 400 s (Fig. 9*C*). Thereby the deceleration of $G\alpha_{i1}$-R178S in multiple turnover measurements can be explained solely by the slowed down single turnover hydrolysis reaction. Due to the change of the rate-limiting step, the slowdown in the multiple turnover assay appears to be only about 2-fold, whereas the single turnover FTIR assay yield the true slowdown by 2 orders of magnitude.

Molecular Dynamics Simulations—To further examine the molecular interactions taking place in the interface between the Ras-like and all-α domain of $G\alpha_{i1}$, molecular dynamics simulations were performed to elucidate the role of Asp^{229} and Asp^{231} at atomic detail. Simulations of wild type $G\alpha_{i1}$ and mutants $G\alpha_{i1}$-D229N and -D231N were performed for 100 ns each. Subsequently contact matrix analysis was carried out for every simulation. Contacts were sampled in time windows of 1 ns and the interaction partners of Asp/Asn^{229} and Asp/Asn^{231} were depicted in Fig. 11. Polar contacts of the side chain groups are indicated by *black bars*.

Asp^{229} formed a stable interdomain contact to the all-α domain through Arg^{242} that bound Gln^{147} in wild type $G\alpha_{i1}$ (Fig. 11*A*). When mutated to Asn^{229}, this interdomain contact triad was interrupted after the first 30 ns. Thereby the contact loss between Asn^{229} and Arg^{242} happened simultaneously to the contact loss of Arg^{242} to Glu^{43} and Gln^{147}. Hence Asp^{229} seems to position Arg^{242} allosterically, so that Arg^{242} forms an interdomain contact that tightly binds and stabilizes the Ras-like and the all-α domain.

Similar to Asp^{229}, Asp^{231} formed an interdomain contact to Arg^{144} within a 100-ns MD simulation (Fig. 11*B*). It is notable, that the contact Asp^{231}-Arg^{144} does neither exist in the starting structure generated from PDB code 1GIA, nor in the original crystal structure, but formed *de novo* in the simulation. The initial contact to Lys^{277} persisted through the simulation time. When mutated to Asn^{231} the initial contact to Lys^{277} was weakened, but the contact to Arg^{144} was completely lost.

Summarizing the results from multiple and single turnover measurements, nucleotide exchange experiments and simulation data, we understand the effects of the point mutations in $G\alpha_{i1}$. $G\alpha_{i1}$-R178S was slowed down in multiple turnover measurements, but even slower in single turnover measurements that depict only the hydrolysis reaction itself. Its nucleotide exchange ability appeared unaltered. Slowdown of multiple turnover is solely from hydrolysis in this case. Thus Arg^{178} only participates in the hydrolysis reaction as described elsewhere (5, 58).

The interface mutations D229N and D231N were both accelerated in multiple turnover measurements. Investigations of the nucleotide exchange reaction showed that the exchange time for both mutants was accelerated. Simulation data suggest an allosteric (Asp^{229}) and direct (Asp^{231}) interdomain binding mode of both amino acids. Mutations affecting the guanosine binding moiety Asp^{272} resulted in accelerated half-life values in multiple turnover measurements that can be originated to an accelerated nucleotide exchange behavior as shown via fluorescence spectroscopy.

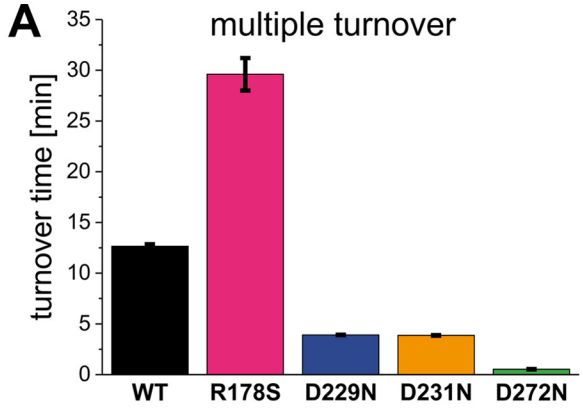

	WT	R178S	D229N	D231N	D272N
turnover time [min]	12.7	29.6	3.9	3.9	0.53
σ [min]	0.18	1.60	0.03	0.03	0.02

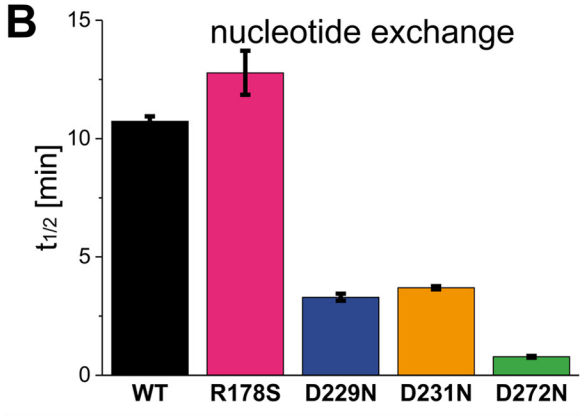

	WT	R178S	D229N	D231N	D272N
$t_{1/2}$ [min]	10.7	12.8	3.3	3.7	0.8
σ [min]	0.21	0.93	0.15	0.07	0.03

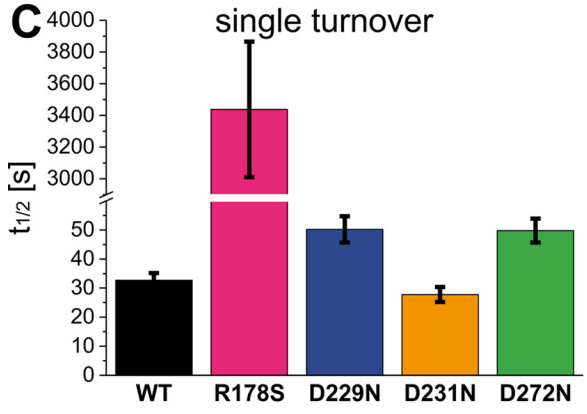

	WT	R178S	D229N	D231N	D272N
$t_{1/2}$ [s]	32.7	3437.7	50.2	27.8	49.8
σ [s]	2.46	426.76	4.47	2.63	4.13

FIGURE 9. Summary of the results of multiple turnover measurements via HPLC at 30 °C (*A*), nucleotide exchange experiments via fluorescence spectroscopy at 30 °C (*B*) and single turnover hydrolysis measurements via FTIR spectroscopy at 15 °C (*C*) of wild type and mutant Gα$_{i1}$.

Discussion

Molecular mechanisms that take place in Gα$_{i1}$ have been investigated by numerous studies including structural (5, 34, 60), computational (61), and biochemical (13, 14, 33) assays. In particular, multiple turnover GTPase assays like malachite green or radiometric phosphate tests using [γ-^{32}P]GTP are widely used even though it is commonly known that GDP/GTP exchange is the rate-limiting step in intrinsic multiple turnover measurements (9–12) and thereby determines k_{obs}. Pre-steady-state measurements using GTP or [γ-^{32}P]GTP pre-loaded Gα subunits that are triggered via Mg^{2+} addition are also able to depict single turnover conditions, but the percentage of nucleotide loading (Gα·GTP *versus* Gα·GDP) and the altered GTP binding affinity due to Mg^{2+}-binding (62) may cause systematic errors such as side reactions like nucleotide exchange. However, in FTIR measurements the percentage of loaded cgGTP *versus* GDP does not influence the kinetics due to the method of phototriggered difference spectroscopy. Additionally we checked the loading rate via HPLC (always >95% cgGTP) and

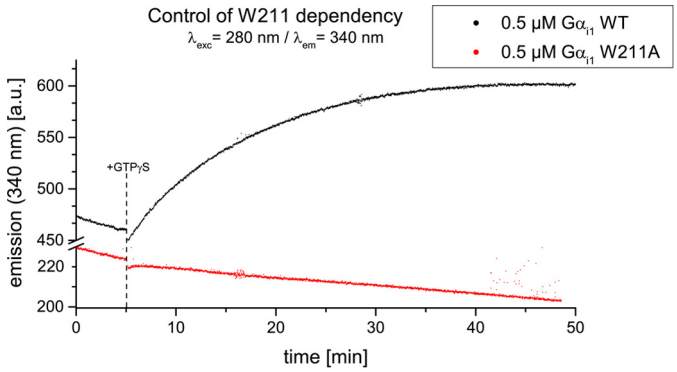

FIGURE 10. **Negative control of the mutant Gα$_{i1}$-W211A in fluorescence spectroscopy.** After baseline monitoring for 5 min, 2.5 μM GTPγS (×5 molar excess) was added to trigger nucleotide exchange.

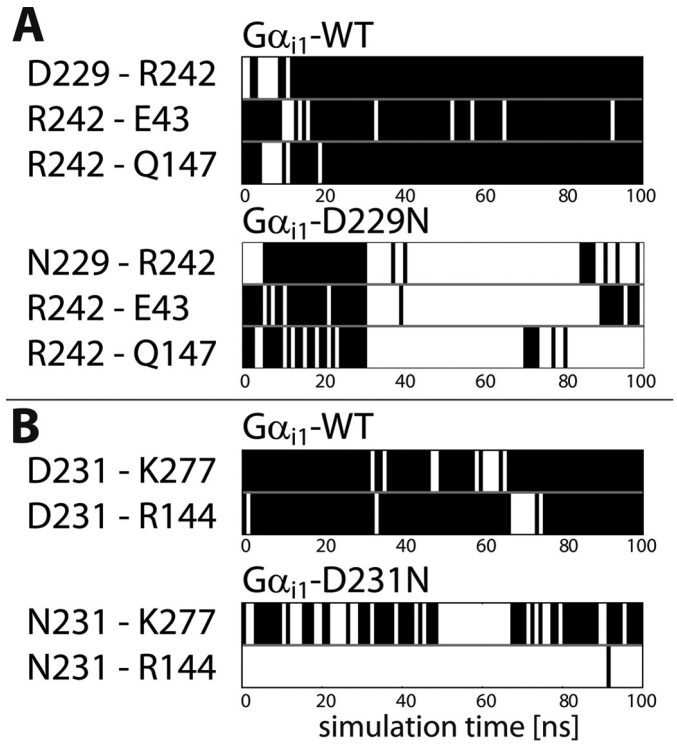

FIGURE 11. **Contact matrix analysis of the molecular interactions taking place in the surrounding of Asp^{229} (*D229*) (WT) and the mutant D229N (*A*) or Asp^{231} (*D231*) (WT) and its mutant D231N (*B*) during a MD simulation.** *Black bars* indicate H-bonds, *white spaces* indicate no H-bond formation.

removed non protein-bound nucleotides. The determined single turnover rate for wild type $G\alpha_{i1}$ measured via FTIR spectroscopy (0.02 s^{-1} at 15 °C) is in good agreement to the literature (0.03 s^{-1} at 30 °C (58) and 0.03 s^{-1} to 0.04 s^{-1} at 20 °C (13, 64)). In addition the ensemble of methods enables a classification of effects caused by point mutations in high detail. Effects caused by the intrinsic arginine finger mutant $G\alpha_{i1}$-R178S were quantified correctly in single turnover measurements (2 orders of magnitude) but not in multiple turnover measurements (factor of 2). The unaltered nucleotide exchange rate of $G\alpha_{i1}$-R178X mutants has already been described elsewhere (5).

Single turnover FTIR spectroscopy unravels for the first time the rate-limiting step of the intrinsic GTP hydrolysis in $G\alpha_{i1}$. Analogue experiments with small GTPases revealed that in some cases the bond breakage and in others the P_i release is rate-limiting (57). For $G\alpha_{i1}$ no protein-bound cleaved phosphate intermediate could be observed, thus bond breakage is the rate-limiting step in this reaction. This is surprising due to the tight coordination of the nucleotide by $G\alpha_{i1}$. The narrow protein environment is still able to release free phosphate to the periphery, probably through a small channel located near the γ-phosphate. The measured IR bands for GTP and GDP are very sensitive to changes in the protein environment and depict for the first time the coordination of the natural nucleotides GDP and GTP in $G\alpha_{i1}$ in contrast to GTP analogues, which were described to have poor affinities for $G\alpha_{i1}$ (65). After we have successfully assigned the α-, β-, γ-, and the free phosphate vibrations it will be possible to assess the effect of point mutations in the binding pocket of $G\alpha_{i1}$ in the future supported by theoretical IR spectra calculation from QM/MM simulations as performed for the small GTPase Ras (66) to further decode the experimental spectra. In addition to the phosphate bands, various bands caused by the protein itself were nicely resolved, which will enable investigations of the hydrolysis mechanism taking place in Gα proteins with improved spatio-temporal resolution. The observed band at 1784 cm^{-1} is the first protonation change observed in GTPases to our knowledge. In fact, heterotrimeric G proteins have been speculated to function as pH sensors (67) and a protonation change close to the surface of $G\alpha_{i1}$ could function as a key player in this reaction.

In addition to the intrinsic GTPase reaction of $G\alpha_{i1}$ we were also able to measure the hydrolysis reaction catalyzed by RGS4 via FTIR spectroscopy. Hydrolysis was thereby accelerated by almost 2 orders of magnitude (Fig. 7). As for intrinsic $G\alpha_{i1}$, bond breakage is the rate-limiting step.

We were able to show with our orchestration of different methods that two point mutations in the $G\alpha_{i1}$ Ras-like/all-α interface ($G\alpha_{i1}$-D229N/$G\alpha_{i1}$-D231N) are able to weaken the coordination in the protein domain interface. Our measurements together with MD simulations demonstrate the importance of the amino acid triad Asp^{229}-Arg^{242}-Gln^{147} for the interface coordination in $G\alpha_{i1}$. Asp^{229} holds Arg^{242} in a position to bridge the interface to Gln^{147}. Investigations on the mutant $G\alpha_{i1}$-R242A confirmed its role (nucleotide exchange: 3.09 ± 0.21 min/single turnover hydrolysis: 32.5 ± 3.5 s) and resulted in similar values as $G\alpha_{i1}$-D229N. In agreement, accelerated nucleotide exchange for $G\alpha_{i1}$-R242A has recently been described for the analogue R243H in $G\alpha_o$ (68). Our findings on the other amino acid in the domain interface, Asp^{231}, suggest a direct binding mode of the side chain of Asp^{231} across the interface to Arg^{144}. This contact is not observable in any of the deposited structures of $G\alpha_{i1}$ in the Protein Data Bank, except structure 4PAQ where the side chain of Arg^{144} is slightly tilted toward Asp^{231} with occupancy of 0.46 (69). In contrast to tightly packed crystal structures, the dynamics of $G\alpha_{i1}$ in our experiments and in our simulations are much more comparable with physiological conditions, so we hereby demonstrate the importance of the salt bridge Asp^{231}-Arg^{144}, which is not observable in the crystal structures. Our findings are summarized in an advanced interface binding model of $G\alpha_{i1}$ as shown in Fig. 12.

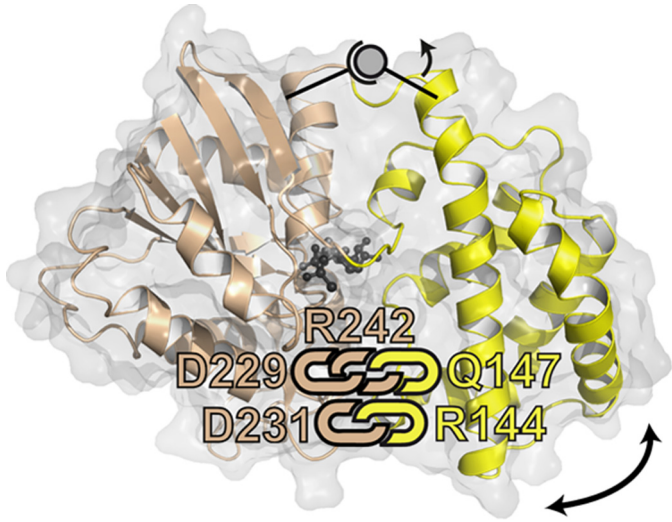

FIGURE 12. **Advanced Ras-like/all-α interdomain binding model of $G\alpha_{i1}$.** In contrast to the crystal structures, Asp^{231} (*D231*) forms an interdomain H-bond to Arg^{144} (*D144*). Arg^{242} (*R242*) is stabilized by Asp^{229} (*D229*) and thereby forms an H-bond to Gln^{147} (*Q147*). Ras-like domain is shown in *beige*, all-α domain in *yellow*, and GTP in *gray balls* and *sticks*.

In summary, we were able to measure the isolated rates of nucleotide exchange and GTP hydrolysis, which both contribute to the signaling state of $G\alpha_{i1}$. In addition we identified the individual phosphate vibrations of GTP, GDP, and P_i during the hydrolysis reaction of $G\alpha_{i1}$. We demonstrated the importance of the intrinsic arginine finger for the hydrolysis reaction and the relevance of Asp^{272} for nucleotide binding. Furthermore, we identified novel key players in the coordination of the Ras-like/all-α interface. Asp^{229} stabilizes the interface allosterically via Arg^{242} and Asp^{231} forms a direct H-bond to Arg^{144}. Orchestration of our methods will further elucidate the molecular mechanisms taking place in $G\alpha_{i1}$ in the future.

Acknowledgments—We thank Prof. Dr. C. H. Wetzel for donation of $G\alpha_{i1}$ cDNA, Dr. Yan Suveyzdis and Jonas Schartner for synthesis of the caged compounds, and Iris Bourdos for excellent technical support.

References

1. Milligan, G., and Kostenis, E. (2006) Heterotrimeric G-proteins: a short history. *Br. J. Pharmacol.* **147,** S46–55
2. Sato, M., Blumer, J. B., Simon, V., and Lanier, S. M. (2006) Accessory proteins for G proteins: partners in signaling. *Annu. Rev. Pharmacol. Toxi-*

col. **46,** 151–187
3. Tall, G. G., Krumins, A. M., and Gilman, A. G. (2003) Mammalian Ric-8A (synembryn) is a heterotrimeric Gα protein guanine nucleotide exchange factor. *J. Biol. Chem.* **278,** 8356–8362
4. Garcia-Marcos, M., Ghosh, P., and Farquhar, M. G. (2009) GIV is a non-receptor GEF for Gαi with a unique motif that regulates Akt signaling. *Proc. Natl. Acad. Sci. U.S.A.* **106,** 3178–3183
5. Coleman, D. E., Berghuis, A. M., Lee, E., Linder, M. E., Gilman, A. G., and Sprang, S. R. (1994) Structures of active conformations of Giα1 and the mechanism of GTP hydrolysis. *Science* **265,** 1405–1412
6. Bokoch, G. M., Katada, T., Northup, J. K., Ui, M., and Gilman, A. G. (1984) Purification and properties of the inhibitory guanine nucleotide-binding regulatory component of adenylate cyclase. *J. Biol. Chem.* **259,** 3560–3567
7. Burns, D. L. (1988) Subunit structure and enzymic activity of pertussis toxin. *Microbiol. Sci.* **5,** 285–287
8. Tesmer, J. J., Berman, D. M., Gilman, A. G., and Sprang, S. R. (1997) Structure of RGS4 bound to AlF4–activated G(iα1): stabilization of the transition state for GTP hydrolysis. *Cell* **89,** 251–261
9. Brandt, D. R., and Ross, E. M. (1986) Catecholamine-stimulated GTPase cycle: multiple sites of regulation by β-adrenergic receptor and Mg^{2+} studied in reconstituted receptor-Gs vesicles. *J. Biol. Chem.* **261,** 1656–1664
10. Birnbaumer, L., Swartz, T. L., Abramowitz, J., Mintz, P. W., and Iyengar, R. (1980) Transient and steady state kinetics of the interaction of guanyl nucleotides with the adenylyl cyclase system from rat liver plasma membranes: interpretation in terms of a simple two-state model. *J. Biol. Chem.* **255,** 3542–3551
11. Levitzki, A. (1980) Slow GDP dissociation from the guanyl nucleotide site of turkey erythrocyte membranes is not the rate limiting step in the activation of adenylate cylase by β-adrenergic receptors. *FEBS Lett.* **115,** 9–10
12. Neer, E. J., and Salter, R. S. (1981) Reconstituted adenylate cyclase from bovine brain: functions of the subunits. *J. Biol. Chem.* **256,** 12102–12107
13. Linder, M. E., Ewald, D. A., Miller, R. J., and Gilman, A. G. (1990) Purification and characterization of $G\alpha_o$ and three types of $G\alpha_i$ after expression in *Escherichia coli*. *J. Biol. Chem.* **265,** 8243–8251
14. Monroy, C. A., Mackie, D. I., and Roman, D. L. (2013) A high throughput screen for RGS proteins using steady state monitoring of free phosphate formation. *PLoS ONE* **8,** e62247
15. Thomas, C. J., Du, X., Li, P., Wang, Y., Ross, E. M., and Sprang, S. R. (2004) Uncoupling conformational change from GTP hydrolysis in a heterotrimeric G protein α-subunit. *Proc. Natl. Acad. Sci. U.S.A.* **101,** 7560–7565
16. Phillips, W. J., and Cerione, R. A. (1988) The intrinsic fluorescence of the α subunit of transducin: measurement of receptor-dependent guanine nucleotide exchange. *J. Biol. Chem.* **263,** 15498–15505
17. Higashijima, T., Ferguson, K. M., Smigel, M. D., and Gilman, A. G. (1987) The effect of GTP and Mg^{2+} on the GTPase activity and the fluorescent properties of G_o. *J. Biol. Chem.* **262,** 757–761
18. Higashijima, T., Ferguson, K. M., Sternweis, P. C., Smigel, M. D., and Gilman, A. G. (1987) Effects of Mg^{2+} and the βγ-subunit complex on the interactions of guanine nucleotides with G proteins. *J. Biol. Chem.* **262,** 762–766
19. Freier, E., Wolf, S., and Gerwert, K. (2011) Proton transfer via a transient linear water-molecule chain in a membrane protein. *Proc. Natl. Acad. Sci. U.S.A.* **108,** 11435–11439
20. Gerwert, K., Freier, E., and Wolf, S. (2014) The role of protein-bound water molecules in microbial rhodopsins. *Biochim. Biophys. Acta* **1837,** 606–613
21. Kuhne, J., Eisenhauer, K., Ritter, E., Hegemann, P., Gerwert, K., and Bartl, F. (2015) Early formation of the ion-conducting pore in channelrhodopsin-2. *Angew. Chem. Int. Ed. Engl.* **54,** 4953–4957
22. Furutani, Y., Fujiwara, K., Kimura, T., Kikukawa, T., Demura, M., and Kandori, H. (2012) Dynamics of dangling bonds of water molecules in pharaonis halorhodopsin during chloride ion transportation. *J. Phys. Chem. Lett.* **3,** 2964–2969
23. Gavriljuk, K., Schartner, J., Itzen, A., Goody, R. S., Gerwert, K., and Kötting, C. (2014) Reaction mechanism of adenylyltransferase DrrA from *Legionella pneumophila* elucidated by time-resolved Fourier transform infrared spectroscopy. *J. Am. Chem. Soc.* **136,** 9338–9345
24. Syberg, F., Suveyzdis, Y., Kötting, C., Gerwert, K., and Hofmann, E. (2012) Time-resolved Fourier transform infrared spectroscopy of the nucleotide-binding domain from the ATP-binding cassette transporter MsbA: ATP hydrolysis is the rate-limiting step in the catalytic cycle. *J. Biol. Chem.* **287,** 23923–23931
25. Völlmecke, C., Kötting, C., Gerwert, K., and Lübben, M. (2009) Spectroscopic investigation of the reaction mechanism of CopB-B, the catalytic fragment from an archaeal thermophilic ATP-driven heavy metal transporter: hydrolytic mechanism of the catalytic CPx-ATPase domain. *FEBS J.* **276,** 6172–6186
26. Troullier, A., Gerwert, K., and Dupont, Y. (1996) A time-resolved Fourier transformed infrared difference spectroscopy study of the sarcoplasmic reticulum Ca^{2+}-ATPase: kinetics of the high-affinity calcium binding at low temperature. *Biophys. J.* **71,** 2970–2983
27. Barth, A., and Mäntele, W. (1998) ATP-induced phosphorylation of the sarcoplasmic reticulum Ca^{2+} ATPase: molecular interpretation of infrared difference spectra. *Biophys. J.* **75,** 538–544
28. Cepus, V., Scheidig, A. J., Goody, R. S., and Gerwert, K. (1998) Time-resolved FTIR studies of the GTPase reaction of H-ras p21 reveal a key role for the β-phosphate. *Biochemistry* **37,** 10263–10271
29. Gavriljuk, K., Gazdag, E.-M., Itzen, A., Kötting, C., Goody, R. S., and Gerwert, K. (2012) Catalytic mechanism of a mammalian Rab·RabGAP complex in atomic detail. *Proc. Natl. Acad. Sci. U.S.A.* **109,** 21348–21353
30. Kötting, C., and Gerwert, K. (2015) What vibrations tell us about GTPases. *Biol. Chem.* **396,** 131–144
31. Kötting, C., Blessenohl, M., Suveyzdis, Y., Goody, R. S., Wittinghofer, A., and Gerwert, K. (2006) A phosphoryl transfer intermediate in the GTPase reaction of Ras in complex with its GTPase-activating protein. *Proc. Natl. Acad. Sci. U.S.A.* **103,** 13911–13916
32. Rudack, T., Xia, F., Schlitter, J., Kötting, C., and Gerwert, K. (2012) Ras and GTPase-activating protein (GAP) drive GTP into a precatalytic state as revealed by combining FTIR and biomolecular simulations. *Proc. Natl. Acad. Sci.* **109,** 15295–15300
33. Hamm, H. E., Meier, S. M., Liao, G., and Preininger, A. M. (2009) Trp fluorescence reveals an activation-dependent cation-π interaction in the Switch II region of $G\alpha_i$ proteins. *Protein Sci.* **18,** 2326–2335
34. Rasmussen, S. G., DeVree, B. T., Zou, Y., Kruse, A. C., Chung, K. Y., Kobilka, T. S., Thian, F. S., Chae, P. S., Pardon, E., Calinski, D., Mathiesen, J. M., Shah, S. T., Lyons, J. A., Caffrey, M., Gellman, S. H., Steyaert, J., Skiniotis, G., Weis, W. I., Sunahara, R. K., and Kobilka, B. K. (2011) Crystal structure of the β_2-adrenergic receptor–Gs protein complex. *Nature* **477,** 549–555
35. Goody, R. S. (1982) A simple and rapid method for the synthesis of nucleoside 5′-monophosphates enriched with ^{17}O or ^{18}O on the phosphate group. *Anal. Biochem.* **119,** 322–324
36. Park, C.-H., and Givens, R. S. (1997) New photoactivated protecting groups: 6. *p*-hydroxyphenacyl, a phototrigger for chemical and biochemical probes. *J. Am. Chem. Soc.* **119,** 2453–2463
37. Hecht, S. M., and Kozarich, J. W. (1973) A chemical synthesis of adenosine 5′-[γ-^{32}P]triphosphate. *Biochim. Biophys. Acta* **331,** 307–309
38. Kaplan, J. H., Forbush, B., 3rd, and Hoffman, J. F. (1978) Rapid photolytic release of adenosine 5′-triphosphate from a protected analog: utilization by the sodium:potassium pump of human red blood cell ghosts. *Biochemistry* **17,** 1929–1935
39. Klasen, K., Hollatz, D., Zielke, S., Gisselmann, G., Hatt, H., and Wetzel, C. H. (2012) The TRPM8 ion channel comprises direct G_q protein-activating capacity. *Pflugers Arch.* **463,** 779–797
40. Hohenfeld, I. P., Wegener, A. A., and Engelhard, M. (1999) Purification of histidine tagged bacteriorhodopsin, pharaonis halorhodopsin and pharaonis sensory rhodopsin II functionally expressed in *Escherichia coli*. *FEBS Lett.* **442,** 198–202
41. Mazzoni, M. R., and Hamm, H. E. (1993) Tryptophan207 is involved in the GTP-dependent conformational switch in the α subunit of the G protein transducin: chymotryptic digestion patterns of the GTPγS and GDP-bound forms. *J. Protein Chem.* **12,** 215–221
42. Faurobert, E., Otto-Bruc, A., Chardin, P., and Chabre, M. (1993) Tryptophan W207 in transducin Tα is the fluorescence sensor of the G protein activation switch and is involved in the effector binding. *EMBO J.* **12,**

4191–4198
43. Hardie, D. G. (ed) (1999) *Protein Phosphorylation: A Practical Approach*, 2nd Ed., Oxford University Press, London
44. Gerwert, K. (2002) Molecular reaction mechanisms of proteins monitored by time-resolved FT-IR difference spectroscopy. in *Handbook of Vibrational Spectroscopy* (Chalmers, J. M., and Griffiths, P. R., eds) pp. 3536–3555, John Wiley & Sons, Ltd., Chichester, UK
45. Höweler, U. (2007) *MAXIMOBY*, CHEOPS, Altenberge, Germany
46. Case, D. A., Babin, V., Berryman, J. T., Betz, R. M., Cai, Q., Cerutti, D. S., Cheatham, T. E., III, Darden, T. A., Duke, R. E., Gohlke, H., Goetz, A. W., Gusarov, S., Homeyer, N., Janowski, P., Kaus, J., Kolossváry, I., Kovalenko, A., Lee, T. S., LeGrand, S., Luchko, T., Luo, R., Madej, B., Merz, K. M., Paesani, F., Roe, D. R., Roitberg, A., Sagui, C., Salomon-Ferrer, R., Seabra, G., Simmerling, C. L., Smith, W., Swails, J., Walker, R. C., Wang, J., Wolf, R. M., Wu, X., and Kollman, P. A. (2014) *AMBER 14*, University of California, San Francisco.
47. Vedani, A., and Huhta, D. W. (1991) Algorithm for the systematic solvation of proteins based on the directionality of hydrogen bonds. *J. Am. Chem. Soc.* **113,** 5860–5862
48. Berendsen, H. J., van der Spoel, D., and van Drunen, R. (1995) GROMACS: A message-passing parallel molecular dynamics implementation. *Comput. Phys. Commun.* **91,** 43–56
49. Hess, B., Kutzner, C., van der Spoel, D., and Lindahl, E. (2008) GROMACS 4: algorithms for highly efficient, load-balanced, and scalable molecular simulation. *J. Chem. Theory Comput.* **4,** 435–447
50. Lindahl, E., Hess, B., and van der Spoel, D. (2001) GROMACS 3.0: a package for molecular simulation and trajectory analysis. *Mol. Model. Annu.* **7,** 306–317
51. Pronk, S., Páll, S., Schulz, R., Larsson, P., Bjelkmar, P., Apostolov, R., Shirts, M. R., Smith, J. C., Kasson, P. M., van der Spoel, D., Hess, B., and Lindahl, E. (2013) GROMACS 4.5: a high-throughput and highly parallel open source molecular simulation toolkit. *Bioinformatics* **29,** 845–854
52. Van der Spoel, D., Lindahl, E., Hess, B., Groenhof, G., Mark, A. E., and Berendsen, H. J. (2005) GROMACS: fast, flexible, and free. *J. Comput. Chem.* **26,** 1701–1718
53. Jorgensen, W. L., and Tirado-Rives, J. (1988) The OPLS potential functions for proteins: energy minimizations for crystals of cyclic peptides and crambin. *J. Am. Chem. Soc.* **110,** 1657–1666
54. Rudack, T., Xia, F., Schlitter, J., Kötting, C., and Gerwert, K. (2012) The role of magnesium for geometry and charge in GTP hydrolysis, revealed by quantum mechanics/molecular mechanics simulations. *Biophys. J.* **103,** 293–302
55. Janert, P. K. (2009) *Gnuplot in Action: Understanding Data with Graphs*, Manning Publication Co., Greenwich, CT
56. Barth, A. (2000) The infrared absorption of amino acid side chains. *Prog. Biophys. Mol. Biol.* **74,** 141–173
57. Kötting, C., and Gerwert, K. (2013) The dynamics of the catalytic site in small GTPases, variations on a common motif. *FEBS Lett.* **587,** 2025–2027
58. Zielinski, T., Kimple, A. J., Hutsell, S. Q., Koeff, M. D., Siderovski, D. P., and Lowery, R. G. (2009) Two Gαi1 rate-modifying mutations act in concert to allow receptor-independent, steady-state measurements of RGS protein activity. *J. Biomol. Screen* **14,** 1195–1206
59. Mukhopadhyay, S., and Ross, E. M. (1999) Rapid GTP binding and hydrolysis by G_q promoted by receptor and GTPase-activating proteins. *Proc. Natl. Acad. Sci. U.S.A.* **96,** 9539–9544
60. Wall, M. A., Coleman, D. E., Lee, E., Iñiguez-Lluhi, J. A., Posner, B. A., Gilman, A. G., and Sprang, S. R. (1995) The structure of the G protein heterotrimer Giα1β1γ2. *Cell* **83,** 1047–1058
61. Louet, M., Martinez, J., and Floquet, N. (2012) GDP release preferentially occurs on the phosphate side in heterotrimeric G-proteins. *PLoS Comput. Biol.* **8,** e1002595
62. Ferguson, K. M., Higashijima, T., Smigel, M. D., and Gilman, A. G. (1986) The influence of bound GDP on the kinetics of guanine nucleotide binding to G proteins. *J. Biol. Chem.* **261,** 7393–7399
63. Baltoumas, F. A., Theodoropoulou, M. C., and Hamodrakas, S. J. (2013) Interactions of the α-subunits of heterotrimeric G-proteins with GPCRs, effectors and RGS proteins: a critical review and analysis of interacting surfaces, conformational shifts, structural diversity and electrostatic potentials. *J. Struct. Biol.* **182,** 209–218
64. Berman, D. M., Wilkie, T. M., and Gilman, A. G. (1996) GAIP and RGS4 are GTPase-activating proteins for the Gi subfamily of G protein α subunits. *Cell* **86,** 445–452
65. Gille, A., and Seifert, R. (2003) Low-affinity interactions of BODIPY-FL-GTPγS and BODIPY-FL-GppNHp with G_i- and G_s-proteins. *Naunyn. Schmiedebergs Arch. Pharmacol.* **368,** 210–215
66. Xia, F., Rudack, T., Kötting, C., Schlitter, J., and Gerwert, K. (2011) The specific vibrational modes of GTP in solution and bound to Ras: a detailed theoretical analysis by QM/MM simulations. *Phys. Chem. Chem. Phys.* **13,** 21451–21460
67. Isom, D. G., Sridharan, V., Baker, R., Clement, S. T., Smalley, D. M., and Dohlman, H. G. (2013) Protons as second messenger regulators of G protein signaling. *Mol. Cell* **51,** 531–538
68. Leyme, A., Marivin, A., Casler, J., Nguyen, L. T., and Garcia-Marcos, M. (2014) Different biochemical properties explain why two equivalent Gα subunit mutants cause unrelated diseases. *J. Biol. Chem.* **289,** 21818–21827
69. Kaya, A. I., Lokits, A. D., Gilbert, J. A., Iverson, T. M., Meiler, J., and Hamm, H. E. (2014) A conserved phenylalanine as a relay between the α5 helix and the GDP binding region of heterotrimeric G_i protein α subunit. *J. Biol. Chem.* **289,** 24475–24487

Molecular Biophysics:

Integration of Fourier Transform Infrared Spectroscopy, Fluorescence Spectroscopy, Steady-state Kinetics and Molecular Dynamics Simulations of G α_{i1} Distinguishes between the GTP Hydrolysis and GDP Release Mechanism

Grit Schröter, Daniel Mann, Carsten Kötting and Klaus Gerwert

J. Biol. Chem. 2015, 290:17085-17095.
doi: 10.1074/jbc.M115.651190 originally published online May 15, 2015